Conduction processes in crystalline Ni_xSi_{1-x} films

1998 J. Phys.: Condens. Matter 10 123

(http://iopscience.iop.org/0953-8984/10/1/014)

J. Phys.: Condens. Matter **10** (1998) 123–134. Printed in the UK PII: S0953-8984(98)86282-6

Conduction processes in crystalline Ni_xSi_{1-x} films

Carmit Segal†, Alexander Gladkikh†, Moshe Pilosof†, Haim Behar†, Mike Witcomb‡ and Ralph Rosenbaum†

† Tel Aviv University, School of Physics and Astronomy, Raymond and Beverly Sackler Faculty of Exact Sciences, Ramat Aviv 69978, Israel

‡ University of Witwatersrand, Electron Microscope Unit, Private Bag 3, Wits 2050, South Africa

Received 23 July 1997, in final form 8 September 1997

Abstract. The electrical conductivity and magnetoconductance (MC) have been measured in crystalline nickel–silicon (c-Ni_xSi_{1-x}) films as a function of nickel content, x. An abrupt decrease in the conductivity is observed at the metal–insulator transition where $x_c \approx$ 13.5 at.% Ni. The discontinuity is explained in terms of a percolation model. Above 4 K, the magnetoconductance (MC) is negative and arises from an electron–electron interaction contribution and a weak-localization contribution involving strong spin–orbit scattering. Below 4 K, the magnetoconductance rapidly becomes positive. These low-temperature MC data can be explained using a model of electrons scattering from superparamagnetic particles, first introduced by Gittleman *et al*.

1. The anomalous magnetoconductance puzzle

Over the last decade numerous investigators have observed in amorphous films a dominating *positive* magnetoconductance (MC), $\Delta\sigma = \sigma(B) - \sigma(0)$, which generally appears at low temperatures below 1 K. In contrast, the MC measurements above 4 K are usually *negative* and can be nicely explained using the electron–electron interaction (EEI) theory and the weak-localization (WL) theory involving strong spin–orbit scattering. Below 4 K, a new scattering process often starts to dominate the negative EEI and WL contributions, producing an effective *positive* magnetoconductance. Some examples are these: amorphous Cr_xGe_{1-x} observed by Heinrich *et al* [1], amorphous Re_xSi_{1-x}:Fe by Vinzelberg *et al* [2], Cr_xSi_{1-x} and $Cr_x(SiO)_{1-x}$ by Vinzelberg *et al* [3], amorphous Ni_xSi_{1-x} by Rosenbaum *et al* [4] and by Abkemeier *et al* [5], amorphous Fe_xGe_{1-x} by Albers and McLachlan [6], granular Ni–SiO_2 films by Gittleman *et al* [7] and in melt-spun granular CoCu by Hickey *et al* [8]. The positive magnetoconductance has gone unexplained with the exception of the interpretations found in the articles of Gittleman *et al* [7] and of Hickey *et al* [8].

2. Theoretical background on the positive magnetoconductance

The theoretical model that most likely explains the positive MC data was suggested years ago by Gittleman *et al* [7]. A few years after the Gittleman publication, Helman and Abeles presented a different model based upon electrons tunnelling between neighbouring grains whose magnetic moments are not parallel [9]. The Helman–Abeles model again incorporated the main argument introduced by Gittleman *et al*. Several years ago, Zhang Shufeng rederived the Gittleman results [10], and, most recently, Wiser advanced the

0953-8984/98/010123+12$19.50

Gittleman theory for the case of very small superparamagnetic (SPM) particles having a *range of particle sizes* [11]. Wiser's theory was motivated by the experimental MC results on granular melt-spun CoCu films investigated by the University of Leeds group [8].

Gittleman *et al* considered a sample consisting of very fine magnetic particles or grains embedded in a nonmagnetic host [7]. If each magnetic particle or grain is ferromagnetic consisting of a single magnetic domain and if its diameter is so small that the direction of its magnetic moment is not fixed in space owing to thermal agitation, the particle is called superparamagnetic, or an SPM particle. In order to have a single domain, the particle diameter usually has to be less than the typical width of a domain wall that separates two neighbouring domains. For example, the typical width of an Ni domain wall is 700 Å [12, 13]. Thus, the Ni particle must have a diameter less than 700 Å to be single domain. If the SPM particles are isolated from one another, there will be no significant coupling between the particles; and in this case, the system behaves like a paramagnetic system of randomly aligned magnetic moments of large magnitudes. Let us define the normalized magnetoresistance $\Delta\rho(B)/\rho(0)$ as

$$\Delta\rho(B)/\rho(0) = [\rho(B) - \rho(0)]/\rho(0) = -\Delta\sigma(B)/\sigma(B) \approx -[\sigma(B) - \sigma(0)]/\sigma(0) \tag{1}$$

provided that $\sigma(0) \approx \sigma(B)$. Gittleman *et al* considered the contribution to $\Delta\rho(B)/\rho(0)$ due to an electron moving from one SPM particle to another. They showed that the probability for the electron to be scattered depends on the degree of correlation between the magnetic moments of neighbouring SPM particles averaged over all configurations. Thus, $\Delta\rho(B)/\rho(0)$ is proportional to $-\langle\mu_1 \cdot \mu_2\rangle$, where μ_1 and μ_2 are the magnetic moments of the initial and final SPM particles that define the path of the scattered electron. For SPM particles, the magnetic field causes partial alignment between μ_1 and μ_2. Therefore it follows that

$$\Delta\rho(B)/\rho(0) \propto -\langle\mu_1 \cdot \mu_2\rangle = -\langle\mu_1 \cdot \hat{B}\rangle\langle\mu_2 \cdot \hat{B}\rangle \tag{2}$$

$$\Delta\rho(B)/\rho(0) \propto -[M(B)]^2 \tag{3}$$

where $\hat{B}$ is a unit vector in the direction of the magnetic field and $M(B)$ is the magnetization. For this reason the data for the magnetoresistance are often compared to a plot of the magnetization squared, if magnetization data are available.

If magnetization data are not available, as is our case, the magnetization might be approximated by the classical Langevin function, $M(x) \propto L(x)$:

$$L(x) = \coth(x) - 1/x \tag{4}$$

where $x = \mu_B g_{eff} B/k_B T$. For large x, $L(x) \to 1$; and for small x, $L(x) \to x/3$. Refer to Sears' book for the derivation of the Langevin function [14]. Thus, the Gittleman derivation suggests that the *magnetoconductance* should be positive and quadratic with small fields and should saturate at high fields. There are two fitting parameters—the effective Landé g_{eff} factor appearing in the argument x and the factor in front of the Langevin function. Thus the magnetoconductance associated with the superparamagnetic particles, $\Delta\sigma_{SPM}$, is:

$$\Delta\sigma_{SPM} = \Delta\sigma_{sat}[L(x)]^2 \tag{5}$$

where $\Delta\sigma_{sat}$ is the high-field saturated MC value obtained from the data.

The above results apply only if all the magnetic particles are SPM. However, if there is a range of particle sizes present in the film, then one can obtain results that are completely different from (5). Wiser has calculated the magnetoresistance for such a sample and found a *linear* variation with the field B [11]; his calculated values for $\Delta\rho(B)/\rho(0)$ are in excellent agreement with data for a melt-spun granular sample of CoCu [8].

The other two theories used in the fitting of the MC data are the 3D electron–electron interaction (EEI) theory that has been well described in the literature [15, 16] and the 3D weak-localization (WL) theory that has been detailed also in the literature [17, 18].

3. Sample preparation and characterization

Twenty *crystalline* Ni_xSi_{1-x} films were produced by heat treating *amorphous* Ni_xSi_{1-x} films in a vacuum cell at 500 °C for two hours and allowing the cell to slowly cool down during one day. If numerous films are to be studied from a particular series, it is important that all the films be heat treated together simultaneously in order to insure that these films have an identical thermal cycling history. The amorphous films had been previously deposited on microscope glass slides that were maintained at room temperature during the evaporation. Details on the fabrication of the amorphous Ni_xSi_{1-x} films can be found in [4] and [19]. The film thicknesses are typically 1000 Å. The nickel contents were determined using EDAX (energy dispersive analysis of x-rays) and Rutherford back-scattering studies.

In order to assure that the transmission electron microscope (TEM) samples had the same structure as the films studied in the transport measurements, the TEM samples were also converted in the same run. The TEM samples were obtained from films evaporated onto photoresist coated glass pieces, that were located adjacent to the substrates used in the conductivity studies. These TEM films were lifted off the glass pieces by dissolving away the photoresist in acetone, and the free films were then floated onto standard copper TEM grid holders that provided mechanical support for these fragile films. Thus, these TEM films had identical fabrication and thermal cycling history as the actual measured films; hence, they should reflect the same structural details that were present in the measured films.

With reference to the converted *crystalline* films, transmission electron microscope studies revealed sharp diffraction rings of crystalline Si and weak diffused rings of the metallic Ni_2Si compound. Dark-field electron microscope pictures suggested that the Si grains are large and on the order of 100 Å to 200 Å. The Ni_2Si structure was not observable, and thus its typical size cannot be ascertained. Thus, these films are composed of large insulating Si grains between which are meandering paths of the conducting Ni_2Si compound. Figure 1 illustrates our proposed structure for the films. As long as there is at least one continuous conducting path of Ni_2Si throughout the sample, the film is probably metallic. When the last path is broken by decreasing the Ni content, the electrons must travel through the Si grains either by thermal activation from the valence band into the conduction band of the Si or via variable-range hopping in the Si in order to transverse from one conducting segment of Ni_2Si to another isolated segment of Ni_2Si.

The magnetoconductance data strongly suggest the presence of magnetic particles. What is the physical origin of the magnetic particles? We speculate on the following explanations. One possibility is segregation of excess magnetic atoms during the thermal conversion step, thus forming small magnetic particles. In our case, this would be small Ni particles. Alternatively, the magnetic atoms could come from magnetic impurities in the glass substrate that diffuse to the glass–film surface during the heat conversion step. For example, our microscope glass slides have 0.045% Fe_2O_3 [20]. Another possibility is the presence of magnetic impurities in the starting materials used for the evaporation of the films [21] or magnetic impurities in the graphite evaporation boats that contained these materials [22]. Lastly, there is the possibility of formation of a magnetic compound during the heat conversion step; for example, Belu-Marian's group suggests that the compound $NiSi_2$ can also form during the heat conversion step, and that this compound is magnetic [23]. We saw no diffraction rings of $NiSi_2$ in our films, suggesting the absence of this compound in

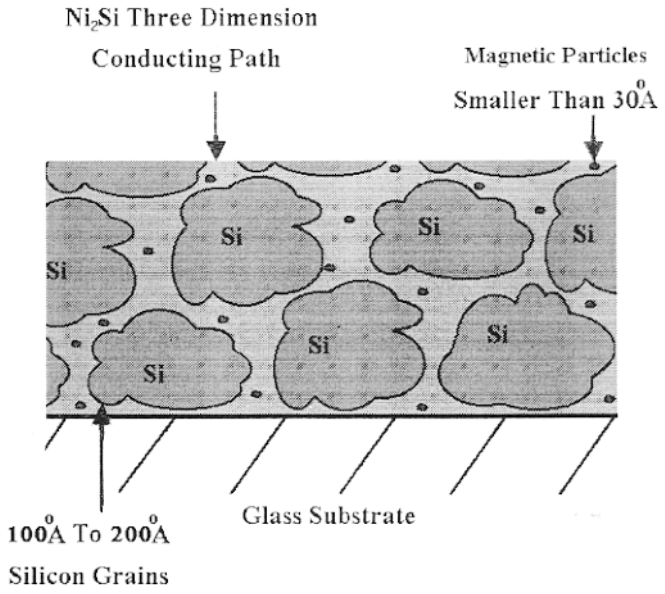

Figure 1. Proposed structure of the crystalline Ni_xSi_{1-x} films based upon TEM studies and magnetoconductance results. The Si grains are excellent insulators; and the electrical connectivity is through the metallic meandering paths of the Ni_2Si compound. Also shown are the magnetic particles or grains that become superparamagnetic below 3 K.

our films. The nickel–silicon phase diagram is quite complex [24]. The presence of these magnetic particles is also included in figure 1.

4. Zero-field conductivity data

The unconverted *amorphous* Ni_xSi_{1-x} films exhibited a smooth continuous decrease in the electrical conductivity as the Ni metal content, x, was decreased [4], as illustrated in figure 2; considerable experimental effort was required to identify the metal–insulator transition which occurred at the critical nickel concentration x_c of 25 at.% Ni in the *amorphous* films [4]. In total contrast, the converted *crystalline* films exhibited a spectacular decrease of the conductivity at a nickel content of about 13.5 at.% Ni, illustrated in figure 2. The jump is on the order of five magnitudes, suggesting the breakage of the last critical backbone (conducting path) in a percolation path model described earlier. Collver reported a critical concentration of 13 atm.% in his films [25, 26]. Similar discontinuous jumps were first observed by Abeles' group many years ago in $W–Al_2O_3$ annealed at 1500 K for 2 hours [27], in $Au–Al_2O_3$ [28] and in $Ag–SiO_2$ [29]. By far the most spectacular jump was recently reported by Wu and McLachlan in a composite system composed of conducting graphite and the very insulating compound boron nitride [30].

Below the MIT at $x_c = 13.5$ at.% Ni, the resistivity of the insulating films exhibited activated hopping where $\rho(T) = \rho_0 \exp(T_0/T)^y$; here T_0 is a characteristic temperature and y is an exponent. For intrinsic conduction (thermal activation of electrons from the valance band to the conduction band) or also for the cases of extrinsic conduction or nearest-neighbour hopping, $y = 1$. For 3D Mott variable-range hopping, $y = \frac{1}{4}$ [31], and for Efros–Shklovskii variable-range hopping, $y = \frac{1}{2}$ [32]. As the resistivities of the insulating films

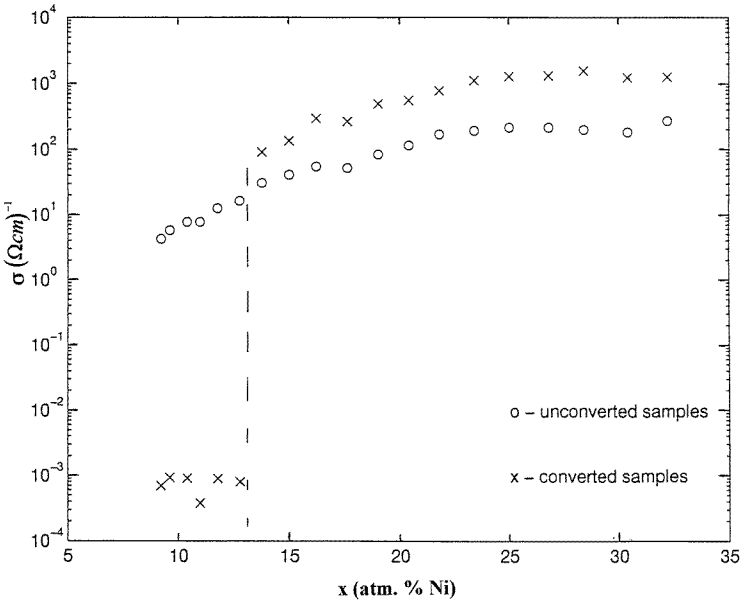

Figure 2. Room-temperature conductivity values versus the nickel content, x. The circles represent the amorphous unconverted nickel–silicon, while the crosses represent the crystalline converted nickel–silicon structure. Notice the discontinuous jump in the conductivity at 13.5 at.% Ni for the converted films.

were so high even at room temperature, only a limited high-temperature span of resistivity measurements between 300 and 800 K was possible. We observed intrinsic conduction with $y = 1$ above 300 K with an energy gap of 0.99 eV, close to that of 1.1 eV reported for crystalline Si [13].

One would anticipate that all the films above the MIT would be metallic. The test that identifies whether the films are metallic or insulating is the parameter w defined as $w = \mathrm{d}\ln\sigma/\mathrm{d}\ln T$; if the film is metallic and its conductivity can be described by the empirical expression $\sigma(T) = \sigma(0) + cT^z$, then $w \to 0$ as $T \to 0$. In contrast, if the film is insulating and displays activated conductivity, then $w \to \infty$ as $T \to 0$. With reference to films having nickel contents greater than 14 at.%, these films had conductivities whose w values tended to extrapolate to zero, thus identifying all these films as metallic. The exception was film No 27 which was barely insulating, and has a nickel content of 13.8 at.%. Thus, the MIT is located slightly above $x_c \approx 14$ at.% Ni. according to the w criterion.

We have fitted the low-temperature conductivity of the metallic films below 4 K to the expression

$$\sigma(T) = \sigma(0) + CT^{1/2} + DT^z \tag{6}$$

where the first term $\sigma(0)$ represents the finite conductivity at absolute temperature, the second term $CT^{1/2}$ is the electron–electron interaction contribution with $C \approx 3\ \mathrm{K}^{-1/2}\ (\Omega\ \mathrm{cm})^{-1}$ [15] and the last term DT^z is an additional scattering process, perhaps arising from the presence of the superparamagnetic particles and/or from weak localization.

Experimentally, we find values of $D = 1.1\ \mathrm{K}^{-3/2}\ (\Omega\ \mathrm{cm})^{-1}$ and $z \approx 3/2$. The fit is shown by the solid line in the inset of figure 3. We have no explanation for this last term;

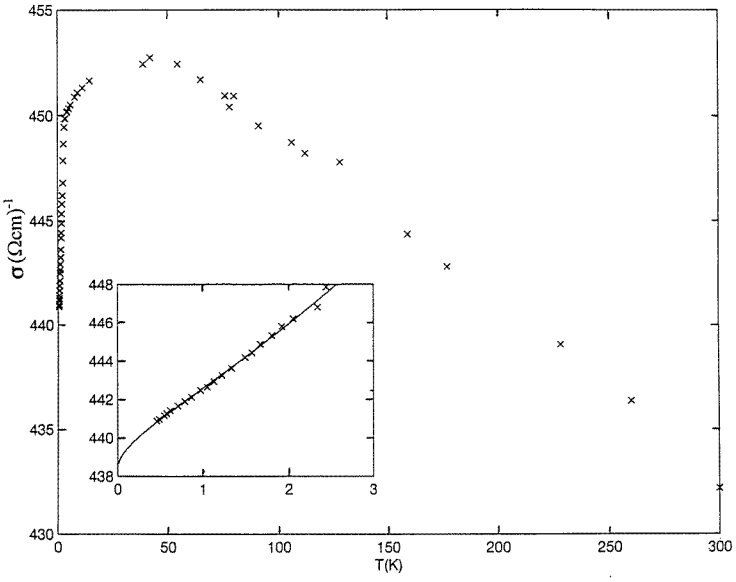

Figure 3. The conductivity of the metallic film having 19 at.% Ni as a function of temperature. The inset displays the low temperature data that are compared to the empirical expression $\sigma(T)\ (\Omega\ \mathrm{cm})^{-1} = 438.4{+}3.2(T/\mathrm{K})^{1/2}{+}1.1(T/\mathrm{K})^{1.55}$. The first term represents the conductivity at absolute zero, $\sigma(0)$. The second term comes from electron–electron interactions. The origin of the third term is not understood. The linear temperature dependence of the conductivity above 50 K comes from electron–phonon scattering.

and we were not successful in fitting a Kondo resistivity term, a $\ln(T_F/T)$ term, to these data [33]. We explain the linear decrease of the conductivity with increasing temperatures observed above 50 K in figure 3 as due to scattering of the electrons from phonons. For temperatures greater than $\Theta_{Debye}/5$, the phonon population of all frequencies is proportional to T. As a result, the temperature correction to the resistivity, $\Delta\rho(T) \propto T$ [34, 35]. As the conductivity $\sigma(T)$ changes little in the high-temperature range between 50 and 300 K as seen in figure 3, we anticipate that $\Delta\sigma(T) \propto -T$ as observed experimentally. The Debye temperature for Ni is 450 K [13].

A fit of (6) to the conductivity data of each metallic film yields a value for $\sigma(0)$, the conductivity at absolute zero. According to the scaling theory that predicts a continuous transition in a 3D system near the MIT owing to disorder, the zero-temperature conductivity, $\sigma(0)$, can be extrapolated to zero according to $\sigma(0) = \sigma_0(x - x_c)^s$ [36]. For our case of strong spin–orbit scattering, the effective critical conductivity exponent, s, is predicted to be $s \approx 1$ [37–39]. The MIT should occur when $\sigma(0)$ vanishes. An extrapolation of the $\sigma(0)$ data versus Ni content in figure 4 indicates a critical concentration $x_c \approx 13$ at.% Ni, consistent with the observed jump in the room-temperature conductivity at 13.5 at.% Ni. The scaling theory prediction should be contrasted with the Mott prediction of a minimum metallic conductivity [40], which is not observed in this system.

5. Magnetoconductance data and comparison to the theories

We had anticipated observing *negative* magnetoconductance (MC) values in crystalline Ni_xSi_{1-x} based upon the *negative* values already observed in the amorphous Ni_xSi_{1-x} films

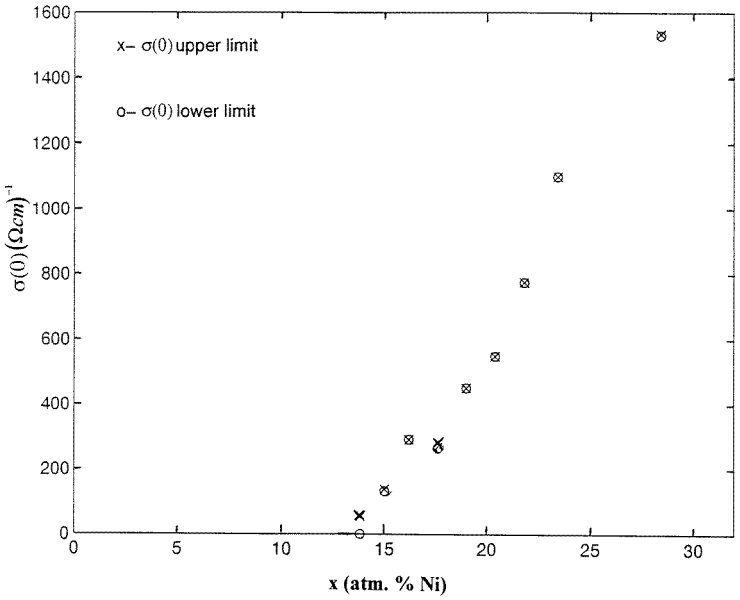

Figure 4. The zero-temperature conductivities versus nickel content, x. Values for $\sigma(0)$ were obtained from empirical fits of equation (6) to the low-temperature conductivity data for the different metallic films. The MIT occurs where $\sigma(0)$ extrapolates to zero, at $x_c \approx 13$ at.% Ni, according to the scaling theory.

[4]. The negative magnitudes arise from a negative contribution from electron–electron interactions (EEIs) [15]:

$$\Delta\sigma_{EEI}(B,T) = -[e^2\tilde{F}_\sigma/(4\pi^2\hbar)][k_BT/(2\hbar D_{diff})]^{1/2}g_3\{g_{eff}\mu_B B/k_BT\} \tag{7}$$

and from the negative weak-localization (WL) contribution involving strong spin–orbit scattering [17, 18]:

$$\Delta\sigma_{WL}(B,T) = \frac{e^2}{2\pi^2\hbar}\sqrt{\frac{eB}{\hbar}}\left[\frac{3}{2}f_3\left(\frac{B}{B_{in}(T)+\frac{4}{3}B_{so}+\frac{2}{3}B_s}\right)-\frac{1}{2}f_3\left(\frac{B}{B_{in}(T)+2B_s}\right)\right]. \tag{8}$$

Analytic expressions for the functions $g_3(x)$ and $f_3(y)$ can be found in references [16] and [18]. The fitting parameters in the EEI expression are the diffusion constant D_{diff}, the electron screening parameter $\tilde{F}_\sigma$ and the effective Landé factor g_{eff}. In the WL expression, the fitting parameters are the temperature-independent effective spin–orbit field B_{so} and the effective magnetic scattering field B_s and the temperature-dependent effective inelastic field $B_{in}(T)$. The relation between the scattering time τ_x and field B_x is given by $\tau_x = \hbar/4eD_{diff}B_x$ [41].

The magnetoconductance of the metallic film No 19 having 19 at.% Ni was compared to the three theories. Above 3.2 K, the MC is negative as illustrated in figure 5, and only the EEI and WL processes contribute. Reasonable values were assigned to the parameters: $D_{diff} = 1 \times 10^{-4}$ m^2 s^{-1}, $g_e = 2$ for the electron Landé factor, $\tilde{F}_\sigma = 0.2$ and the effective magnetic scattering field $B_s = 0$. The inelastic field $B_{in}(T)$ was a free fitting parameter as well as the temperature-independent spin–orbit field B_{so}; B_{so} took on the value of 1.19 T. Note that the spin–orbit field is large corresponding to strong scattering with a typical time of $\tau_{so} \approx 1.3 \times 10^{-12}$ s. The data of figure 5 represent the WL contribution only, where

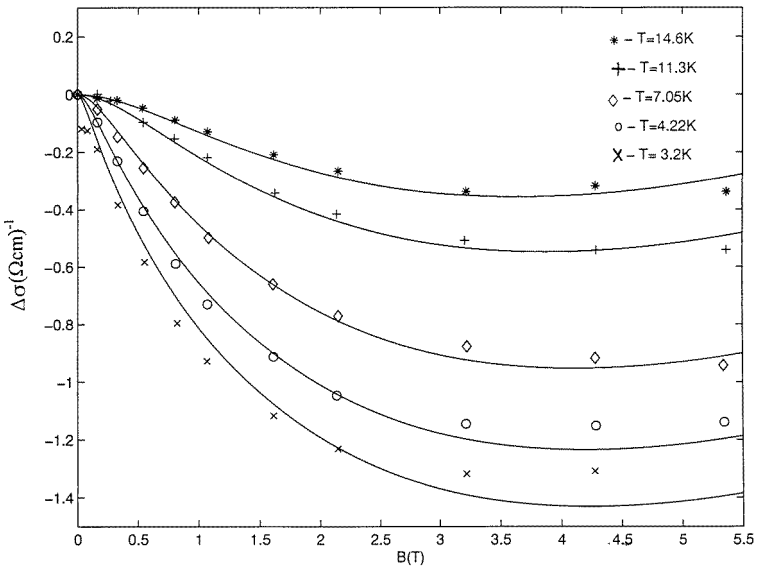

Figure 5. Fits of the weak-localization theory to the magnetoconductance data at 3.2 K and above for the metallic film having 19 at.% Ni. The small negative EEI contribution has already been subtracted from the original data. Notice the negative MC magnitudes, arising from the weak-localization contribution which includes strong spin–orbit scattering. The fitting parameter—the *temperature-independent* spin–orbit effective field B_{so}—is large and equal to the constant value of 1.91 T. The *temperature-dependent* inelastic field $B_{in}(T)$ is treated as the only variable fitting parameter to the different curves.

the very small EEI contribution has already been subtracted from the raw MC data. The solid lines in figure 5 are fits of the WL theory only. The resulting values for the inelastic effective field $B_{in}(T)$ and the inelastic scattering time $\tau_{in}(T)$ are presented in figures 6(a) and 6(b).

The magnetoconductance rapidly changes its behaviour below 3 K as shown in figure 7. The MC data suggest that a new process 'turns on' below 3 K and completely dominates the EEI and WL terms. At 0.5 K, the MC is now positive, increasing very rapidly in magnitude at small fields of a few hundred Gauss and then tending to saturation at higher fields. In order to analyse the data, we assume that this new scattering process works independently of the EEI and WL terms, and hence the negative EEI and WL terms can be approximated in magnitude and subtracted from the data to leave only estimated values for the MC of this new process. By extrapolating values for the effective inelastic field $B_{in}(T)$ to temperatures below 3 K from figure 6(a), the WL term to the MC can be estimated. The contribution from the EEI term can be directly calculated. The resulting MC data with the Wl and EEI contributions subtracted are shown in figure 8. Owing to the saturation behaviour at higher fields for these MC data and its positive sign, the data suggested to us a connection to magnetization behaviour, also observed in [42].

We believe that the Curie temperature T_C for most of our magnetic particles is 3 K. Above 3 K, the particles are paramagnetic and have negligible influence on the conductivity and magnetoconductance; below 3 K, these particles are superparamagnetic.

According to (5), the positive MC can be fitted to the expression $\Delta\sigma_{SPM}(B) = \Delta\sigma_{sat}(T)L^2(x)$, where $L(x)$ is the Langevin function, $\Delta\sigma_{sat}(T)$ is the saturated MC at

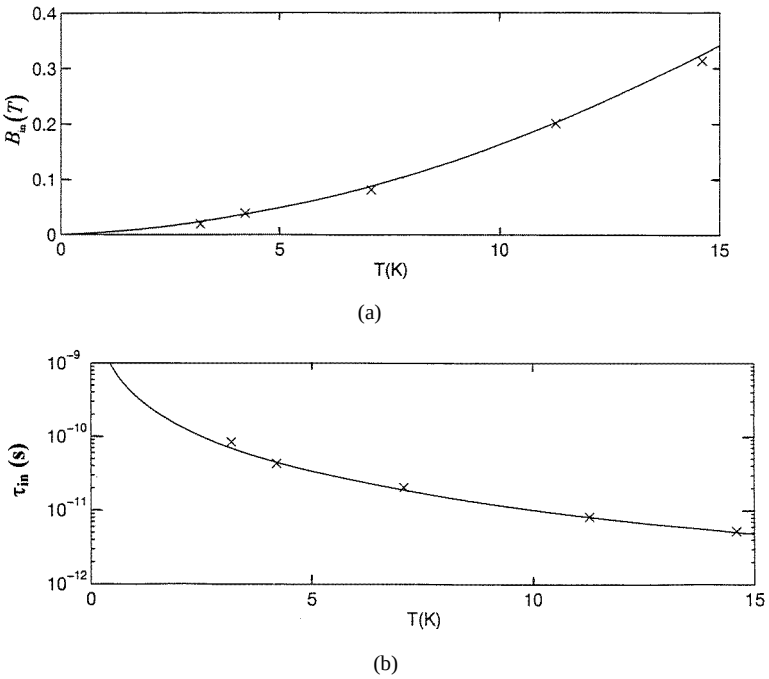

Figure 6. Extracted values for (a) the effective inelastic field $B_{in}(T)$ and (b) the inelastic scattering time $\tau_{in}(T)$ obtained from the fits to the MC data of figure 5.

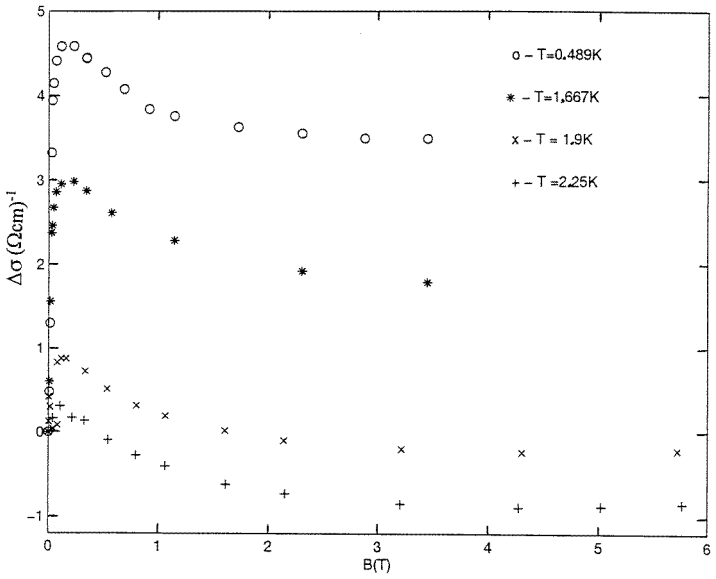

Figure 7. The magnetoconductance (MC) data below 3 K as a function of applied field for the metallic film having 19 at.% Ni. Notice the positive sign of the MC as well as the rapid rise of the MC at very low fields and the tendency of the MC to saturate at high fields.

high fields and $x = g_{eff}\mu_B B/k_B T$. The values for the saturated MC, $\Delta\sigma_{sat}(T)$, can be estimated from the curves of figure 8. The only fitting parameter is the effective Landé

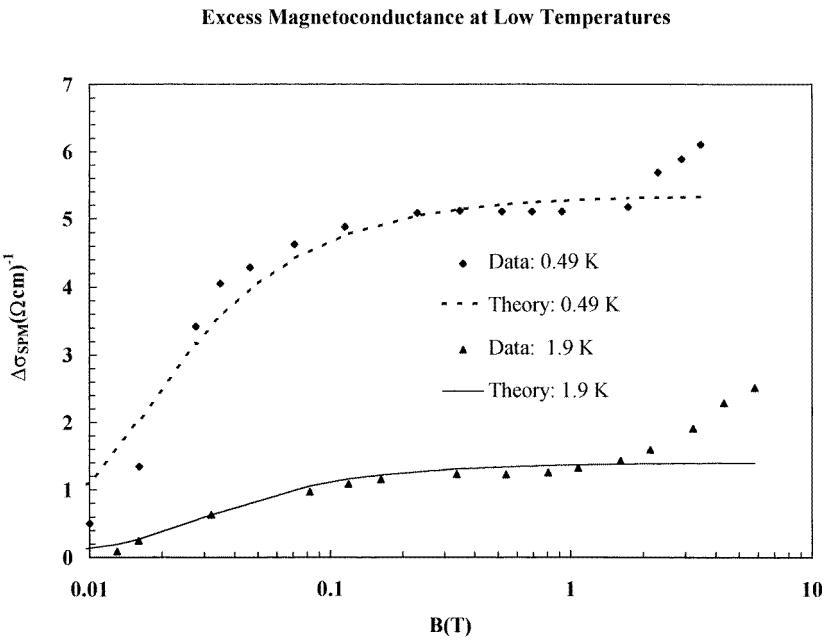

Figure 8. Experimental values for the excess magnetoconductance $\Delta\sigma_{SPM}(B)$, where the electron–electron interaction contribution and the weak-localization contribution have been subtracted from the 0.49 K and 1.9 K data of figure 7. The lines are fits using $\sigma_{sat}[L(x)]^2$, where $L(x)$ is the Langevin function that approximates the magnetization and $x = g_{eff}\mu_B B/k_B T$. The fits are based upon a model of electron scattering from superparamagnetic particles, suggested by Gittleman *et al*.

factor g_{eff} which took on a typical value of 130. The dashed line fit to the MC data at $T = 0.49$ K in figure 8 is acceptable using the Langevin function approximation to the magnetization. Both the B^2 behaviour of the MC at low fields and the saturation of the MC are reproduced. The saturation behaviour occurs at fields greater than 0.1 Tesla. However, there are inconsistencies at higher temperatures. For example the theory predicts that at the higher temperature of 1.667 K, the saturation behaviour should occur at higher fields of approximately 0.3 Tesla. This prediction is not observed in the MC data at 1.667 K in figure 7 and might be associated with different Curie temperatures for the various particles in this transition region. Moreover an effective Landé g_{eff} of 265 was required to fit the 1.9 K MC data. It would be useful to extend the MC to lower temperatures where one would anticipate saturation at even smaller fields (less than 0.1 Tesla).

Since the Landé g factor for nickel is 0.60 [43], a typical superparamagnetic particle having an effective Landé factor g_{eff} of 130 would be composed of about 220 nickel atoms. Using an interatomic distance of 2.49 Å for a Ni atom [12], 220 nickel atoms would be fitted into a particle or grain having a diameter of 15 Å. If the moment arises from the $NiSi_2$ compound rather than Ni atoms and if the unit cell of $NiSi_2$ has a larger diameter of 5.5 Å and perhaps the typical g factor of $\approx$2, then the typical particle diameter would be 22 Å. A particle smaller than 30 Å is too small to be observed in our transmission electron microscope. For evaluating (1), typical values for $\sigma(T = 0.49\ \text{K}, B = 0)$ and $\sigma(T = 1.67\ \text{K}, B = 0)$ are 453.206 and 457.195 $(\Omega\ \text{cm})^{-1}$ for the $x = 19$ at.% Ni film.

The very small diameters of the SPM particles are expected to directly influence their physical properties. First, the Curie temperature T_C should be greatly reduced. Recall that the Curie temperature is directly proportional to the exchange constant, J. If the particle is small, most of the atoms reside on the surface rather than in the bulk, and hence the effective exchange constant, J, should be greatly reduced. For example, Beckmann and Bergmann report that two Ni atoms are barely magnetic [44, 45]; in support of this claim are the magnetoconductance results of Lin *et al* [46] which suggest that Ni particles having diameters smaller than 6 Å are nonmagnetic, which implies that $T_C = 0$. In contrast, bulk Ni has a $T_C = 627$ K [13]. Thus for very small-diameter Ni particles, there must be a rapid decrease of $T_C \to 0$; this argument might explain our low Curie temperatures of $T_C \approx 3$ K. Secondly, there are preferred orientation directions of the magnetic moment of the SPM particle along certain crystallographic directions. In our case the unit cell is probably that of Ni or $NiSi_2$. The magnetic moment is randomly oriented only if the anistropy energy is less than thermal energy k_BT. Since the anistropy energy scales directly with the volume of the particle [13], there will be no preferred alignment direction of the moment for very small-diameter particles. This argument probably explains why the magnetic field required to produce the saturated positive magnetoconductance is so small in magnitude. In addition, the large magnetic moment of the SPM particle also contributes to the effect.

In conclusion, we claim that the positive magnetoconductance values observed below 3 K arise from electrons scattering off the moments of very small-diameter superparamagnetic particles.

Acknowledgments

We are grateful to Professors Guy Deutscher, Roman Mints, N Wiser and Y Korenblit, to Drs A Milner and A Gerber and to Mr B Groisman for fruitful discussions. Much helpful computer assistance came from Miss Irit Opher. We acknowledge the generous funding from the German–Israeli Foundation (GIF) and from the Tel Aviv University Research Fund.

References

[1] Heinrich A, Vinzelberg H, Elefant D and Gladun C 1993 *Non-Cryst. Solids* **164–166** 513
[2] Vinzelberg H, Heinrich A, Metz C and Schumann J 1996 *Preprint*
[3] Vinzelberg H, Heinrich A, Gladun C and Schumann J 1994 *Hopping and Related Phenomena* ed C J Adkins, A R Long and J A McInnes (Singapore: World Scientific) p 266
[4] Rosenbaum R *et al* 1994 *J. Phys.: Condens. Matter* **9** 5395
[5] Abkemeier K M, Adkins, C J, Asal R and Davies E A 1992 *J. Phys.: Condens. Matter* **4** 9113
[6] Albers A and McLachlan D S 1993 *J. Phys.: Condens. Matter* **5** 6067
[7] Gittleman J I, Goldstein Y and Bozowski S 1972 *Phys. Rev.* B **5** 3609
[8] Hickey B J, Howson M A, Musa S O and Wiser N 1995 *Phys. Rev.* B **51** 667
[9] Helman J S and Abeles B 1976 *Phys. Rev. Lett.* **37** 1429
[10] Zhang Shufeng 1992 *Appl. Phys. Lett.* **61** 1855
[11] Wiser N 1996 *J. Magn. Magn. Mater.* **159** 119
[12] Cullity B D 1972 *Introduction to Magnetic Materials* (Reading, MA: Addison-Wesley) ch 11
[13] Kittel C 1971 *Introduction to Solid State Physics* (New York: Wiley) p 490
[14] Sears F W 1969 *Introduction to Thermodynamics, The Kinetic Theory of Gases and Statistical Mechanics* (Reading, MA: Addison-Wesley) p 307
[15] Lee P A and Ramakrishnan T V 1985 *Rev. Mod. Phys.* **57** 308
[16] Ousset J C, Askenazy S, Rakoto H and Broto J M 1985 *J. Physique* **46** 2145
[17] Fukuyama H and Hoshino K 1981 *J. Phys. Soc. Japan* **50** 2131
[18] Baxter D V, Richter R, Trudeau M L, Cochrane R W and Strom-Olsen J O 1989 *J. Physique* **50** 1673
[19] Rosenbaum R, Heines A, Karpovski M, Pilosof M and Witcomb M 1997 *J. Phys.: Condens. Matter* **9** 5411

[20] Blue Star Micro Slides BS 3836-1974 manufactured by Chance Propper, Span Lane, Smethwick, Warley, West Midlands B6C 1NZ, UK
[21] Nickel metal 99.97% pure and silicon pieces 99.999% pure: Cerac, 407 N 13th Street, Milwaukee, WI 53233, USA
[22] EB4 graphite E-Beam crucibles: Poco Graphite, 1601 S State Street, Decatur, TX 76234, USA
[23] Belu-Marian A, Serbanescu M D, Manaila R and Devenyi A 1995 *Appl. Surf. Sci.* **91** 63
[24] Hansen M and Anderko K 1958 *Constitution of Binary Alloys* (New York: McGraw-Hill) p 1040
[25] Collver M M 1977 *Solid State Commun.* **23** 333
[26] Collver M M 1978 *Appl. Phys. Lett.* **32** 574
[27] Abeles B, Pinch H L and Gittleman J I 1975 *Phys. Rev. Lett.* **35** 247
[28] Abeles B, Sheng P, Coutts M D and Arie Y 1975 *Adv. Phys.* **24** 407
[29] Priestley E B, Abeles, B and Cohen R W 1975 *Phys. Rev.* B **12** 2121
[30] Wu Junjie and McLachlin D S 1997 *Phys. Rev.* B **56** 1236
[31] Mott N F 1968 J. *Non-Cryst. Solids* **1** 1
[32] Efros A L and Shkovskii B I 1975 *J. Phys.: Solid State Phys.* **8** L49
[33] Abrikosov A A 1972 *Introduction to the Theory of Normal Metals (Solid State Physics Series supplement 12)* ed H Ehrenreich, F Seitz and D Turnbull (New York: Academic) p 78
[34] Ziman J M 1963 *Electrons and Phonons* (Oxford: Claredon) p 365
[35] Blakemore J S 1974 *Solid State Physics* (Philadelphia, PA: Saunders) p 188
[36] Abrahams E, Anderson P W, Licciardello D C and Ramakrishnan T V 1979 *Phys. Rev. Lett.* **42** 693
[37] Belitz D and Kirkpatrick T R 1994 *Rev. Mod. Phys.* **66** 322
[38] Nishida N, Furubayashi T, Yamaguchi M, Morigaki K and Ishimoto H 1985 *Solid State Electron.* **28** 81
[39] Yoshizumi S, Mael D, Geballe T H and Greene R L 1985 *Localization and Metal–Insulator Transitions* ed H Fritzsche and D Adler (New York: Plenum) p 81
[40] Mott N F 1972 *Phil. Mag.* **26** 1015
[41] Bergmann G 1984 *Phys. Rep.* **107** 30
[42] Gerber A, Milner A, Groisman B, Karpovsky M, Gladkikh A and Sulpice A 1997 *Phys. Rev.* B **55** 6446
[43] Weast R C (ed) 1968 *Handbook of Chemistry and Physics* (Cleveland, OH: Chemical Rubber Company) p E-117
[44] Beckmann H and Bergmann G 1996 *Phys. Rev.* B **54** 368
[45] Bergmann G 1978 *Phys. Rev. Lett.* **41** 264
[46] Lin J J, Jian W B, Yamada R and Kobayashi S 1996 *Int. Conf. on Electron Localization and Quantum Transport in Solids (Warsaw, 1996)* abstract booklet, p 135